Thermodynamics of the Hydrolysis of Lithium Salts: Pathways to the Precipitation of Inorganic SEI Components in Li-Ion Batteries

Journal of The Electrochemical Society, 2021 **168** 100514

Thermodynamics of the Hydrolysis of Lithium Salts: Pathways to the Precipitation of Inorganic SEI Components in Li-Ion Batteries

Simone Di Muzio,[1] Annalisa Paolone,[1] and Sergio Brutti[1,2,3,*,z]

[1]*Consiglio Nazionale delle Ricerche, Istituto dei Sistemi Complessi, 00185 Rome, Italy*
[2]*Sapienza University of Rome, Department of Chemistry, 00185 Rome, Italy*
[3]*GISEL-Centro di Riferimento Nazionale per i Sistemi di Accumulo Elettrochimico di Energia, 50121 Firenze, Italy*

Here we discuss the thermodynamics of the hydrolysis of four fluorinated lithium salts widely used in aprotic electrolytes for lithium-ion batteries: lithium hexafluorophosphate ($LiPF_6$), lithium bis(trifluoromethylsulfoyl)imide (LiTFSI), lithium bis (fluorosulfonyl)imide (LiFSI) and the hybrid salt lithium fluorosulfonyl-trifluorofulfonyl imide (LiFTFSI). We performed density functional theory calculations at the B3LYP/6–31++G** level of theory using an implicit solvation model, to derive the electronic structures, vibrational properties and the thermodynamic stability of reagents, reaction intermediates and hydrolysis products. We combined ab initio thermodynamic evaluations in solution with thermochemical cycles to derive the variation of the Gibbs energy of heterogeneous reactions, where the precipitation of solid products is considered. Our analysis has been performed at three different temperatures to investigate the possible influence of the temperature on the formation of the reaction products. Overall, the use of imide-based anions limits the spontaneous hydrolysis, by hindering the formation of POF_3 differently from $LiPF_6$. All FSI- TFSI- and FTFSI-hydrolyses lead to the precipitation of solid LiOH and, to a lesser extent, of solid LiF. In comparison with other salts, LiTFSI apparently holds down more efficiently the precipitation of solid LiF and limits the onset of the self-feeding salt degradation mechanisms.

 [DOI: 10.1149/1945-7111/ac2aca]

Manuscript submitted August 2, 2021; revised manuscript received September 13, 2021. Published October 8, 2021.

Supplementary material for this article is available online

The hydrolysis of lithium salts in aprotic electrolytes plays a key role in the degradation chemistry in Li-ion batteries (LIBs).[1–6] Thus, in order, to enhance the battery life, mitigation strategies have been developed mainly by minimizing the amount of free water in the electrolytes through sequestration by electrode fillers[6,7] or functional separators.[8,9]

Among all lithium salts used in LIBs,[10–15] lithium hexafluorophosphate ($LiPF_6$) is by large the most common thanks to its optimal balancing between chemical, thermal and electrochemical stability, toxicity and safety, compared to $LiClO_4$, $LiAsF_6$, $LiBF_4$ and $LiSO_3CF_3$.[16,17] Other lithium salts like lithium bis(oxalate) borate (LiBOB),[18] lithium bis(trifluoromethylsulfoyl)imide (LiTFSI)[19] and lithium bis(fluorosulfonyl)imide (LiFSI)[20] have also been proposed and studied in the research literature to improve sustainability and hazard mitigation. Hydrolysis in all cases is an issue[20] as the presence of the inevitable water traces opens the door to parasitic chemical recations[1,17,21–26] and alters the composition and stability of the solid electrolyte interphases (SEI) spontaneously grown over the electrode surfaces.[2,5,11] In fact, like all the other electrolyte components (i.e. solvent blend, soluble additives), lithium salts participate to the sequence of irreversible reactions occurring spontaneously between electrolyte and electrodes, both in open circuit conditions (chemical reactivity) and upon polarization (electrochemical reactivity).[5,27,28] The most detrimental parasitic process involving the highly-fluorinated lithium salts is the release of HF, that is highly reactive and aggressive towards the positive electrodes and the counter collectors.[29–34]

Experimental and computational studies about the spontaneous reactivity of lithium salts in LIBs with water have been reported by many authors, focusing mainly on the kinetics of HF release and the reactivity with the solvent molecules (i.e. organic carbonates or ethers).[1,21–25,29,31] Reaction mechanisms have been proposed based on experimental or computational evidences[29,31] but the thermodynamics of these processes remains unclear. The methodological aspect that mainly limits the comprehension of the thermodynamics of these chemical reactions deals with the complexity of these multiphase and multicomponent systems: both experimentally and computationally it is not easy to identify and decouple the impact of the major specific homogeneous or heterogeneous reactions and quantify the underlying thermodynamic quantities (i.e. Gibbs energies of reaction and equilibrium constants).

In this study we tackle the thermodynamic description at various temperatures of the hydrolysis of $LiPF_6$, LiFSI, LiTFSI and the hybrid salt lithium fluorosulfonyl-trifluorofulfonyl imide (LiFTFSI) by electronic structure calculations by density functional theory (DFT) performed in a simulated solvent: the chemical structure of these salts is presented in Fig. 1. Here we also apply thermodynamic cycles to combine the ab initio thermodynamic descriptions of reactions in the solvent media with the precipitation of insoluble LiF (s) and LiOH(s). Our aim is to describe how the hydrolysis of these lithium salts onsets the nucleation of SEI components on electrodes through spontaneous chemical paths driven by the favourable reaction thermodynamics.

Our study starts from the state-of-the-art salts widely adopted in commercial Li-ion battery formulations, i.e. $LiPF_6$: its hydrolysis has been studied before and here we compare our prediction with previous reports. Starting from the consensus concerning the hydrolysis of lithium hexafluorophosphate, we propose hydrolysis mechanisms for LFSI, LiTFSI and LiFTFSI in analogy to $LiPF_6$, considering the inevitable changes and adaptations. As far as we know, this is the first study to report a comparative analysis of the hydrolysis of imide-based lithium salts using $LiPF_6$ as benchmark.

Methods

Electronic structure calculations by DFT have been performed by using the Spartan18 software[35]: the hybrid functional B3LYP[36] has been adopted with the 6–31++G** basis set.[37] The choice of the B3LYP/6–31++G** method has been made to balance between computational costs and the accuracy. Stereo-conformers have been identified by exploiting molecular mechanics routines embedded in the Spartan18 software. Equilibrium geometries for all molecules and conformers have been obtained by full structural relaxations of the atomic positions. Solvation has been simulated by adopting an

*Electrochemical Society Member.
[z]E-mail: sergio.brutti@uniroma1.it

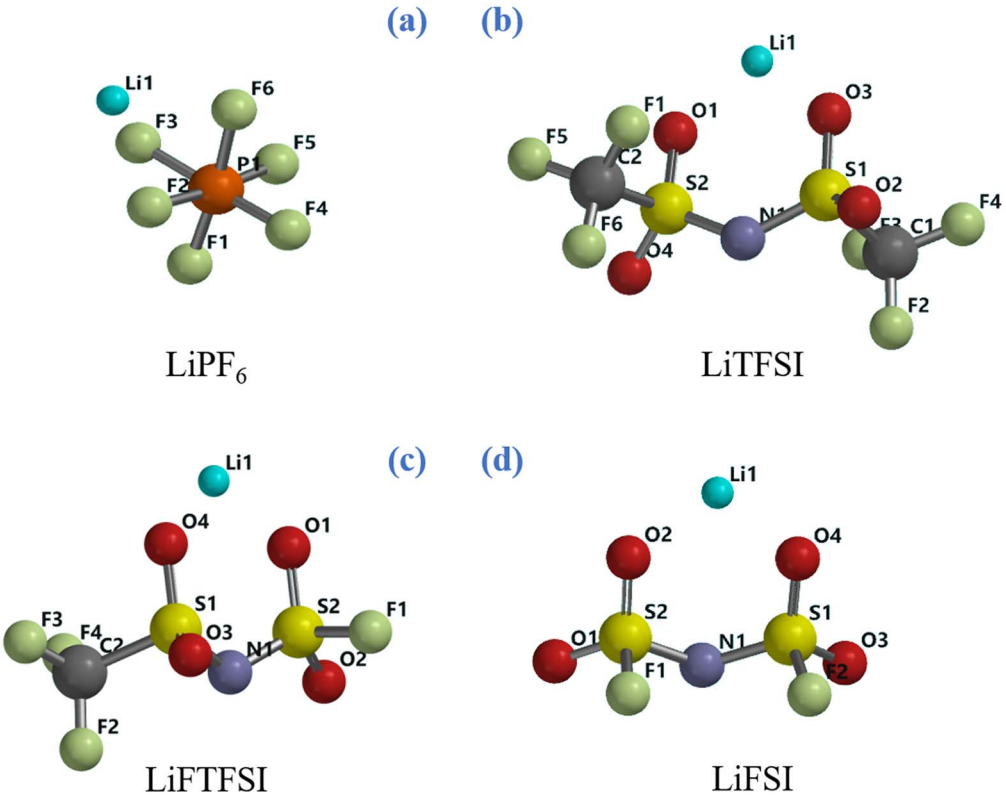

Figure 1. Chemical structures of the four lithium salts: (a) lithium hexafluorophosphate; (b) lithium bis(trifluoromethylsulfonyl)imide; (c) lithium fluorosulfonlyl-trifluoromethylsulfonyl imide; (d) bis(fluorosulfonyl) imide.

implicit solvation model (Polarizable Continuum Model, PCM[38]) mimicking a polar environment ($\varepsilon = 37.22$). Vibrational frequencies and zero-point energies have been computed for all chemical species. The total Gibbs energies of a generic molecular species *i* (either neutral or charged) have been calculated at various temperatures, i.e. $G_T^{tot,DFT}(i)$, by evaluating the corresponding partition functions and considering zero-point energies. Isolated atoms and monatomic ions thermodynamics have been computed using Gaussian09 package[39] adopting the same level of theory. Free Gibbs Energy of reactions have been calculated as stoichiometrically-weighed differences between Gibbs Free Energy products or intermediates and reactants.

The computational accuracy of the adopted B3LYP/6–31++G** method has been evaluated by comparing the thermodynamics of selected reactions with similar calculations performed by more advanced functionals (M06–2X/6–31++G**; ωB97X-D/6–31++G**)[40,41] or methods at higher level of theory (MP2/6–31++G**), assuming in all cases the same basis set.[42] Two reactions have been considered in vacuum, namely (a) $LiPF_6 \rightarrow LiF$

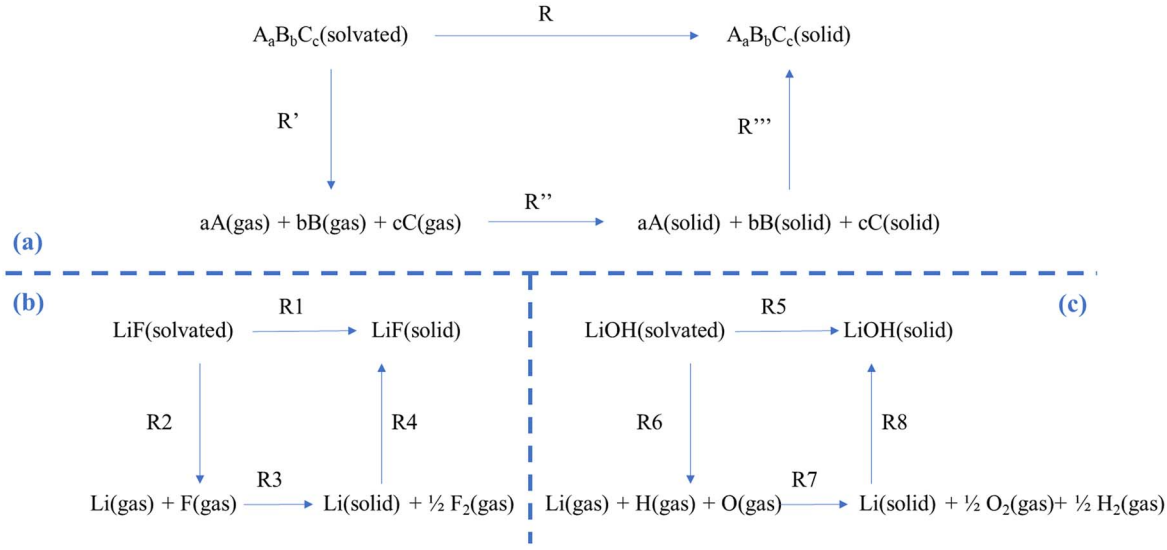

Figure 2. (a) General reactions cycle suitable to evaluate any thermodynamic quantity related to the precipitation reaction (R) of a general substance $A_aB_bC_c$. (b) Reaction cycle for the evaluation of the precipitation thermodynamics of LiF(s); (c) Reaction cycle for the evaluation of the precipitation thermodynamics of LiOH(s).

Table I. Thermodynamic equations necessary to derive the Gibbs energies of the precipitation reaction of the generic substance $A_aB_bC_c$ from computational and literature data. $G_T^{tot,DFT}(i((j))$ is the computational DFT total Gibbs energy of the generic specie *i* in the state *j*at a given temperature T, $\Delta_f G_T^o(i(gas))$ is the formation Gibbs energy at the same temperature T of the monatomic gas *i* retrieved from the literature databases as well as the $\Delta_f G_T^o(A_aB_bC_c(solid))$ that is the Gibbs energy of formation of the solid specie $A_aB_bC_c$.

Reactions	
$\Delta_r G_T^o(R) = \Delta_r G_T^o(R') + \Delta_r G_T^o(R'') + \Delta_r G_T^o(R''')$	(R)
Atomization reaction of $A_aB_bC_c$(solvated)	
$\Delta_r G_T^o(R') = a\Delta G_T^{tot,DFT}(A(gas)) + b\Delta G_T^{tot,DFT}(B(gas))$ $+c\Delta G_T^{tot,DFT}(C(gas)) - G_T^{tot,DFT}(A_aB_bC_c(solvated))$	(R')
Formation reaction of the monatomic gas	
$\Delta_r G_T^o(R'') = a\cdot\Delta_f G_T^o(A(gas)) + b\cdot\Delta_f G_T^o(B(gas))$ $+c\cdot\Delta_f G_T^o(C(gas))$	(R')
Formation reaction of the $A_aB_bC_c$(solid)	
$\Delta_r G_T^o(R''') = \Delta_f G_T^o(A_aB_bC_c(solid))$	(R'')

+ PF_5 and (b) $LiPF_6 + H_2O \rightarrow HF + LiOH + PF_5$. The corresponding Gibbs energy of reaction at 298 K in vacuum are:

- Reaction (a): 130, 147, 172, 147 kJ mol^{-1} for B3LYP, ωB97X-D, M06–2X and MP2, respectively.
- Reaction (b): 210, 228, 237, 229 kJ mol^{-1} for B3LYP, ωB97X-D, M06–2X and MP2, respectively.

The relative accuracy of the three functionals in respect to the benchmark MP2 method have been calculated as average between the two relative calculated errors; the final estimated relative errors are: 9.9, 0.1 and 10.3% for B3LYP, ωB97X-D andM06–2X, respectively. Apart from the outperforming and computationally expensive ωB97X-D functional, B3LYP and M06–2X show a similar computational accuracy. In the view of a balanced compromise between computational costs and accuracy we adopted B3LYP.

To evaluate the thermodynamic of heterogeneous reactions leading to the precipitation of LiF(s) and LiOH(s), we considered the thermodynamic cycles shown in Fig. 2. Cycles have been drawn by modifying an approach already used by us for oxides, peroxides and superoxides for aprotic lithium oxygen batteries[43]

The precipitation thermodynamics of a generic substance $A_aB_bC_c$ can be derived by combining computational data on molecules, either solvated or in the gas phase, obtained by electronic structure calculations or similar methods, with assessed literature thermodynamic quantities.[44] By assuming the generic thermodynamic cycle shown in Fig. 2a, one may calculate the Gibbs energy of reaction R, $\Delta_r G_T^o(R)$, by the equations summarized in Table I.

Turning to the precipitation of LiOH(s) and LiF(s), we can derive the corresponding Gibbs energy of precipitation (reactions R1 and R5) by the following equations:

$$\Delta_r G_T^o(R1) = [G_T^{tot,DFT}(Li(gas)) + G_T^{tot,DFT}(O(gas)) + G_T^{tot,DFT}(H(gas)) - G_T^{tot,DFT}(LiOH(solvated))] + [\Delta_f G_T^o(Li(gas)) + \Delta_f G_T^o(O(gas)) + \Delta_f G_T^o(H(gas))] + [\Delta_f G_T^o(LiOH(solid))] \quad [1]$$

$$\Delta_r G_T^o(R5) = [G_T^{tot,DFT}(Li(gas)) + G_T^{tot,DFT}(F(gas)) - G_T^{tot,DFT}(LiF(solvated))] + [\Delta_f G_T^o(Li(gas)) + \Delta_f G_T^o(F(gas))] + [\Delta_f G_T^o(LiF(solid))] \quad [2]$$

being all symbols defined in line to the caption of Table I. By using this approach, it is possible to evaluate the thermodynamics of the same reaction paths at different temperatures by retrieving the correct literature data from the database [44] and computing DFT Gibbs total energies at the same temperature. All supporting thermodynamic data collected from the literature are reported in the supplementary information (SI) Table SI.

Results

$LiPF_6$ hydrolysis in simulated aprotic media.—Li^+ is strongly coordinated by the PF_6^- anion in the simulated solvent through electrostatic interactions with the partial negative charges of three fluorine atoms. Following the atomic labels shown in Fig. 1, the interatomic distances are Li1—F3 = 2.007 Å, Li1—F2 = 2.028 Å, Li1—F6 = 2.015 Å being the Li1—P1 distance 2.575 Å.

It is widely known that $LiPF_6$ undergoes in aprotic solvents two competitive dissociation reactions:[45–48]

$$LiPF_6 \rightleftarrows Li^+ + PF_6^- \quad [3]$$

$$LiPF_6 \rightleftarrows PF_5 + LiF \quad [4]$$

being the first the usual ionic dissociation and the second a Lewis acid/base equilibrium. The calculated Gibbs energy of both reactions at 298 K are positive, i.e.64 kJ mol^{-1} and 92 kJ mol^{-1}, respectively. The ionic dissociation of reaction 3 is driven by the solvation of Li^+ ions in dielectric media[48] whereas reaction 4 is negligible below 60 °C in consideration to the large values of free reaction energy. This last equilibrium is commonly considered as the onset reaction of the thermal aging of $LiPF_6$-based electrolytes in presence of traces of water. In fact, above 60 °C the PF_5 molecule easily react with water giving:

$$PF_5 + H_2O \rightleftarrows POF_3 + 2HF \quad [5]$$

Our calculations suggest for 5 a Gibbs energy of reaction at 298 K of −51 kJ mol^{-1}. In the literature many authors reported that at room temperature 5 is slow, and the consensus suggests a $LiPF_6$ limited degradation through the formation of LiF:[45,46]

$$LiPF_6 + H_2O \rightleftarrows POF_3 + 2HF + LiF \quad [6]$$

being our computational prediction for the corresponding Gibbs energy of reactionat 298 K $\Delta_r G_{298K}^o(E6) = 41$ kJ mol^{-1}.

Besides these known mechanisms, one can also speculate that $LiPF_6$ can react with water and irreversibly break in fragments leading to the release of LiOH through an Arrhenius acid/base equilibrium in solution:

$$LiPF_6 + H_2O \rightleftarrows PF_5 + HF + LiOH \quad [7]$$

The formation of HPF_6 is excluded since it is vibrationally unstable and spontaneously evolves in a coordinated adduct $PF_5\cdots HF$, constituted by two weakly interacting fragments. Overall, the computed thermodynamics of this process is very endergonic ($\Delta_r G_{298K}^o(E7) = 186$ kJ mol^{-1} at 298 K) and it is unlikely to occur. Generally speaking, the thermodynamic landscape of the hydrolysis of $LiPF_6$ in solution outlined from our calculation does not clarify the strong tendency of this solvated salt to easily degrade in presence of traces of water.

A different picture can be drawn by considering the precipitation of solid LiOH(s) and LiF(s). In Fig. 3 the potential energy surface (PES) of the hydrolysis mechanism of lithium hexafluorophosphate considering the precipitation of solids is shown at three different temperatures. These heterogeneous reaction channels show smaller or even negative energy barriers and therefore are thermodynamically feasible in the 248–348 K temperature range:

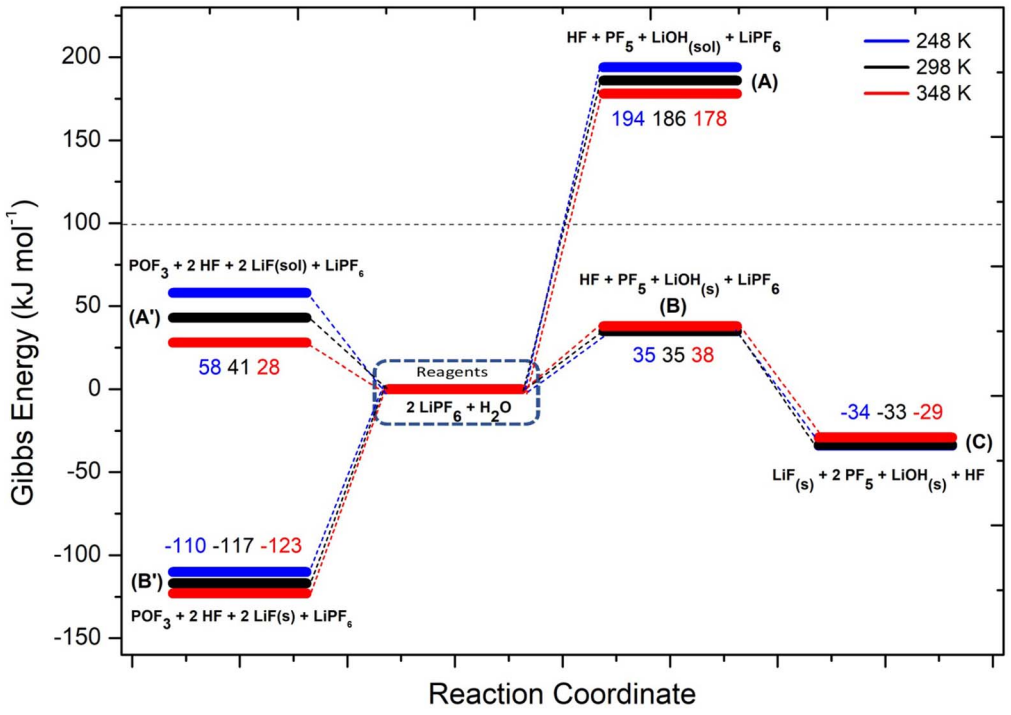

Figure 3. Potential Energy Surface for $LiPF_6$ hydrolysis reaction (numerical values are the energy differences in respect to the reagents at the various temperatures).

$$LiPF_6 + H_2O \rightleftarrows PF_5 + HF + LiOH\,(s) \qquad [7b]$$

$$LiPF_6 + H_2O \rightleftarrows POF_3 + 2HF + LiF\,(s) \qquad [8]$$

$$2LiPF_6 + H_2O \rightleftarrows 2PF_5 + HF + LiOH\,(s) + LiF\,(s) \qquad [9]$$

being the corresponding Gibbs energies of reaction at 298 K 35, –117 and −68 kJ mol^{-1}, respectively. On passing, one can note that the precipitation of LiOH(s) as a first hydrolysis products decrease the Gibbs energy of reaction from 186 (7) to 35 kJ mol^{-1} (7b) at 298 K: this energy barrier is therefore small enough to start the $LiPF_6$ hydrolysis at room temperature observed experimentally.[45,46] Overall, this thermodynamic path nicely matches with the experimental evidence in model studies[45,46] as well as the reported presence of oxofluorides, LiOH(s) and LiF(s) in the composition of passivation films grown over negative electrodes in aprotic LIBs.[27]

The summary of the $\Delta_r G_T^o$ values for reactions involved in the hydrolysis of $LiPF_6$ are reported in the SI, Table SII.

LiFSI hydrolysis in simulated aprotic media.—Li^+ cation is coordinated by FSI^- anion in simulated aprotic solvent via electrostatic interactions with partial negative charges of O2 and O4 atoms (see Fig. 1). Following the atomic labels depicted in Fig. 1, the interatomic distances Li1—O_2 and Li1—O_4 are identical (1.88 Å) and the value of angle S2-N1-S1 is 122°. The two fluorine atoms and computed structure of LiFSI are in *syn* configuration.

In Fig. 4 the potential energy surface (PES) of the hydrolysis mechanism of LiFSI is shown.

This reaction pathway starts with the acid/base equilibrium between LiFSI and water (10–11):

$$LiFSI + H_2O \rightleftarrows HFSI + LiOH\,(s) \qquad [10]$$

$$LiFSI + H_2O \rightleftarrows HFSI + LiOH\,(sol) \qquad [11]$$

The precipitation of LiOH drives the thermodynamics, being the computed Gibbs reaction energy to give solid lithium hydroxide (10) 13 kJ mol^{-1} at 298 K, whereas the reaction to the solvated LiOH (sol) (11) has a $\Delta_r G^o_{298K}(E11)$ = 164 kJ mol^{-1} at 298 K.This different thermodynamic landscape suggests that LiFSI can react with water leading to the precipitation of lithium hydroxide and forming HFSI, especially for temperatures below 298 K.

The structure of HFSI is shown in the SI, Fig. S1 (available online at stacks.iop.org/JES/168/100514/mmedia); it can react again through reaction (12):

$$HFSI \rightleftarrows FNO_4S_2 + HF \qquad [12]$$

This reaction is endergonic and consists in the neutral loss of hydrofluoric acid from HFSI. The main product of the 12 reaction is the molecular fragment FNO_4S_2 (see SI, Fig. S1). The minimal energy barrier to climb to activate this process is as high as 43–57 kJ mol^{-1}, in respect to the reagent molecule (HFSI). This value is high enough to expect a limited reactivity through this channel, even smaller if large activation barriers occur. Therefore, in comparison to $LiPF_6$ hydrolysis, LiFSI is less prone to release HF. On the other hand, the equilibrium of the overall hydrolysis shifts to the products side including in the reactive pathway also reaction (13):

$$LiFSI + HF \rightleftarrows HFSI + LiF\,(s) \qquad [13]$$

This reaction is strongly exergonic with a computed $\Delta_r G^o_{298K}(E13)$ = −90 kJ mol^{-1} at 298 K and likely drives a shift of the overall equilibrium in favour of the hydrolysis products. It is to be noted that the precipitation of LiF(s) results in the release of another HFSI molecule that can react again, through reaction (12), thus opening the door to a self-feeding process.

Turning to the effect of temperature, the hydrolysis of LiFSI is enhanced at low temperature being favoured the precipitation of solid products.

The summary of the $\Delta_r G_T^o$ values for reactions involved in the hydrolysis of LiFSI are reported in the SI, Table SIII.

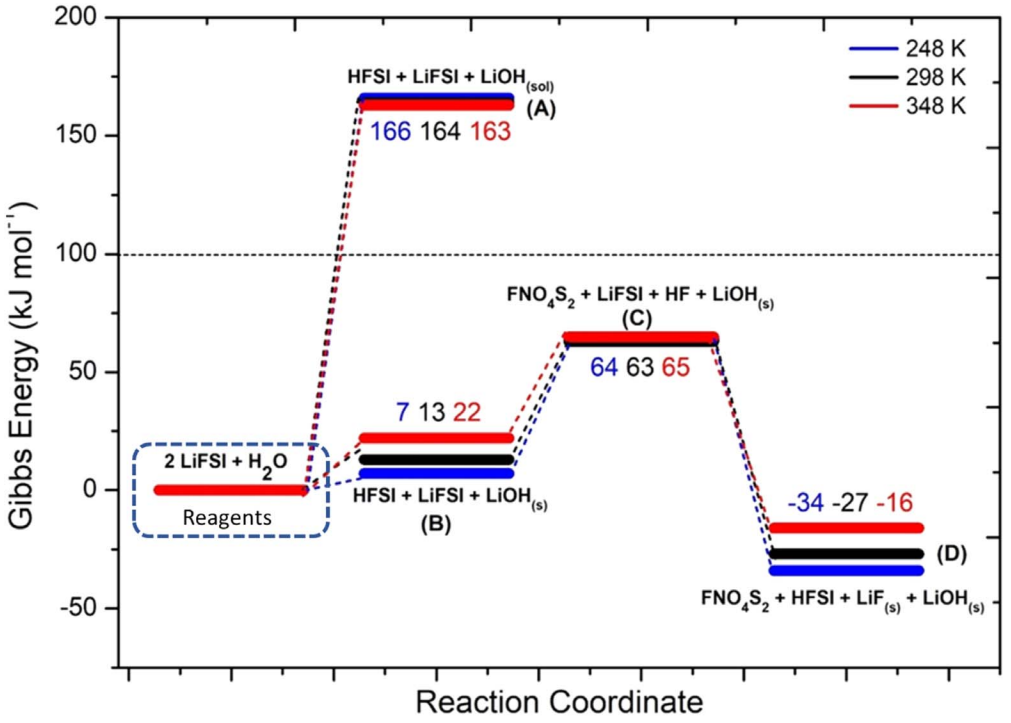

Figure 4. Potential Energy Surface for LiFSI hydrolysis reaction (numerical values are the energy differences in respect to the initial state: i.e. 2LiFSI + H_2O at the various temperatures).

LiTFSI hydrolysis in simulated aprotic media.—Li^+ cation is coordinated by the $TFSI^-$ anion by coulombic interactions between the positively charged metal ion and the negatively charged sulphonyl groups: the distances between Li1-O1 and L1-O2 are both 1.60 Å (see Fig. 1). Both trifluoromethyl groups are in the *anti* configuration. In Fig. 5 the potential energy surface (PES) of the LiTFSI hydrolysis process is displayed.

Also in this case, the hydrolysis begins with the acid/base equilibrium between LiTFSI and water:

$$LiTFSI + H_2O \rightleftarrows HTFSI + LiOH\,(s) \quad [14]$$

$$LiTFSI + H_2O \rightleftarrows HTFSI + LiOH\,(sol) \quad [15]$$

Like $LiPF_6$ and LiFSI, the precipitation of solid lithium hydroxide leads to a Gibbs energy of reaction 14 of 13 kJ mol^{-1} at 298 K, approximately 150 kJ mol^{-1} smaller compared to the formation of solvated LiOH(sol).

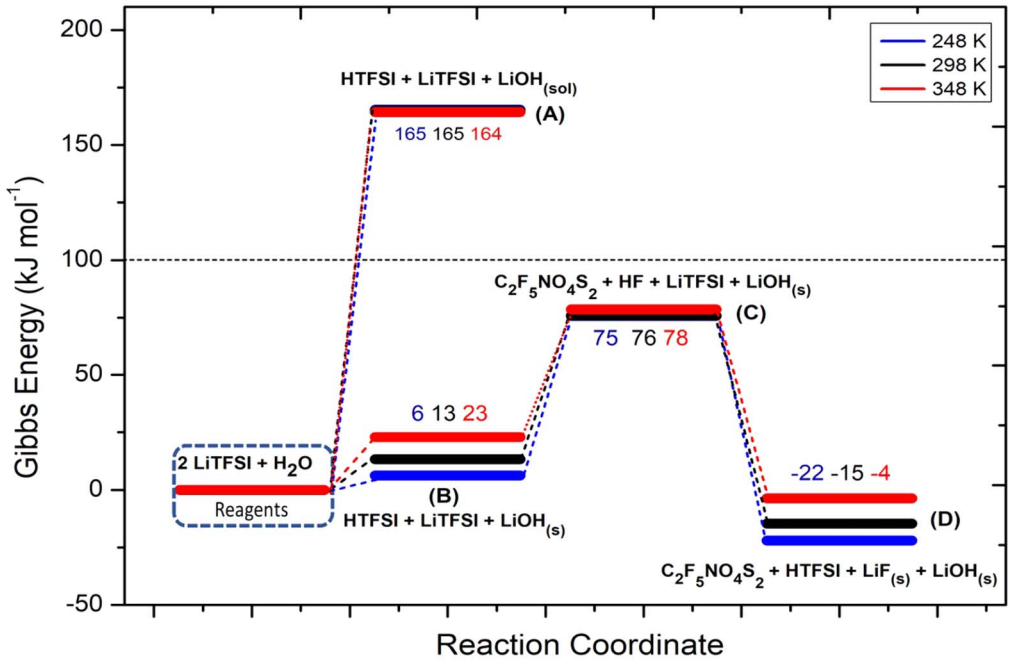

Figure 5. Potential Energy Surface (PES) for the LiTFSI hydrolysis reaction at three temperatures (numerical values are the energy differences in respect to the initial state: i.e. 2LiTFSI + H_2O at the various temperatures).

The precipitation of lithium hydroxide occurs in parallel to the formation of the solvated acid HTFSI, being its structure shown in the SI, Fig. S2. The proton is coordinated by the electron pair on the nitrogen atom.

The release of hydrofluoric acid starting from HTFSI through reaction 16 is an endergonic reaction:

$$HTFSI \rightleftarrows C_2F_5NO_4S_2 + HF \quad [16]$$

The abstraction of a fluorine atom from $-CF_3$ is thermodynamically expensive due to the strength of the covalent C–F bond. The structure of the fragment molecule $C_2F_5NO_4S_2$ released in reaction 16 is shown in the SI, Fig. S2. Being the energy barrier to release HF as high as 63 kJ mol^{-1} at room temperature in respect to HTFSI, this path is unlikely to occur also in consideration of the additional energy costs due to the possible kinetic activation energies and reaction 15 (i.e. 13 kJ mol^{-1} at 298 K). Overall HF release by hydrolysis is likely strongly limited in the case of LiTFSI, in comparison to LiFSI and $LiPF_6$.

Again, the thermodynamics of the overall hydrolysis is shifted towards the products by the strongly exergonic character of reaction 17:

$$LiTFSI + HF \rightleftarrows HTFSI + LiF(s) \quad [17]$$

The computed Gibbs energy of reaction 17 is -91kJ mol^{-1}, leading to a final product blend constituted by LiF(s)+LiOH(s)+HTFSI(sol)+$C_2F_5NO_4S_2$(sol). Also in this case, the final HTFSI molecule can react again through reactions 16–17 opening also in this case a self-feeding reaction channel.

The summary of the $\Delta_r G_T^o$ values for reactions involved in the hydrolysis of LiTFSI are reported in the SI, Table SIV.

LiFTFSI hydrolysis in simulated aprotic media.—Li^+ is coordinated to $FTFSI^-$ anion trough electrostatic interaction between Li cation and partial negative charges on oxygen atoms (see Fig. 1). The distance between Li1 and O4 is 1.86 Å and the distances between Li1 and O2 is 1.88 Å.This ionic couple is asymmetric due to the different substitution of sulphur atoms: S2 atom is linked to two oxygens and one fluorine atom (F1) while S1 is connected totwo oxygens and one CF_3 group. In Fig. 6 the potential energy surface (PES) for the LiFTFSI hydrolysis mechanism is shown.

The hydrolysis of LiFTFSI starts from the acid/base equilibrium between LiFTFSI and water, as described in reactions 18 and 19:

$$LiFTFSI + H_2O \rightleftarrows HFTFSI + LiOH(s) \quad [18]$$

$$LiFTFSI + H_2O \rightleftarrows HFTFSI + LiOH(sol) \quad [19]$$

As expected, the precipitation of lithium hydroxide drives the thermodynamics with a Gibbs reaction energy for 18 of 15 kJ mol^{-1} at 298 K; on the contrary $\Delta_r G^o_{298K}(E19)$, where LiOH is solvated, is 166 kJ mol^{-1}.

The structure of the acid HFTFSI is shown in the SI, Fig. S3. Following the general scheme already outlined for the FSI and the TFSI anions, HFTFSI can break in fragments to release hydrofluoric acid following the reaction 20:

$$HFTFSI \rightleftarrows CF_3NO_4S_2 + HF \quad [20]$$

The Gibbs reaction energy of 20 is 46 kJ mol^{-1} at 298 K, a value very close to reaction 12. This value is expected since the HF release originates from the cleavage of the S–F bond, like in reaction 12, differently from the more expensive break of the C–F bond in reaction 16 (see above). The other reaction product of 20 is the fragment molecule $CF_3NO_4S_2$: its molecular structure is shown in the SI, Fig. S3.

Overall, the combination of reaction 18 and 20 leads to an energy barrier of 61 kJ mol^{-1} (thermodynamic limit), without considering the kinetic activation energies. This threshold matches the similar path of the FSI-hydrolysis (i.e. reactions 10–12), whereas it is 15 kJ mol^{-1} smaller compared to the combined path of the HF release (14–16) from LiTFSI. Once formed, the HF molecule can easily react with LiFTFSI to give solid LiF(s) following reaction 21:

$$LiFTFSI + HF \rightleftarrows HFTFSI + LiF(s) \quad [21]$$

This reaction is exergonic and $\Delta_r G^o_{298K}(E21) = -89$ kJ mol^{-1} at 298 K and leads to the release of HFTFSI, that can feed back reaction 20 and thus possibly opens the door to a chain reactivity.

The summary of the $\Delta_r G_T^o$ values for reactions involved in the hydrolysis of LiFTFSI are reported in the SI, Table SV.

Imide based salts vs lithium hexafluorophosphate.—The comparison among the various hydrolysis mechanisms here proposed allow to identify three main common reaction steps:

1. The LiOH(s) precipitation;
2. The HF release;
3. The LiF(s) precipitation.

The comparison of the Gibbs reaction energies at 298 K is shown in the Fig. 7 for these three main reaction steps.

All imide-based salts show an energy barrier below 15 kJ mol^{-1} at room temperature for the formation of LiOH(s). On the other hand, the HF release is strongly endergonic for all lithium imides being the corresponding $\Delta_r G^o_{298K} > 50$ kJ mol^{-1}. The final hydrolysis step, that also feedback the process (see above) is the LiF(s) precipitation that is in all cases strongly exergonic, therefore driving the overall hydrolysis. In this respected $LiPF_6$ is a compromise, as in reaction 7b the precipitation of LiOH(s) and the HF release are simultaneous: the corresponding Gibbs energy of reaction is larger compared to all the LiOH(s) from imides, whereas it is smaller compared to HF release from imides.

The different thermodynamic landscape of the hydrolysis of imides compared to $LiPF_6$ necessarily impact the chemical nature of the native passivation layer over electrodes grown in aprotic lithium batteries. In fact, the inorganic phases formed during the hydrolysis can accumulate over the electrodes starting the accumulation of the SEI even in open circuit conditions. Overall, the use of imide-based lithium salts likely leads to LiOH(s)-richer SEI layer over electrodes but likely hinders a massive accumulation of LiF(s) due to the strongly endergonic HF release steps, especially in the case of LiTFSI. A SEI richer in LiOH(s) and poorer in LiF(s) is expected to facilitate the lithium ionic mobility from and into the electrode active material thank to the larger ionic conductivities.[27] On passing it is important to underline that SEI grown on negative electrodes or passivation films deposited on positive electrodes are the results of the complex interplay between the chemically driven salt hydrolysis (that is the goal of this study), the electrochemical degradation of the electrolyte constituents (solvents, additives, salts), and the spontaneous reactivity of soluble and insoluble chemical species (electrolyte components as well as byproducts originating from degradations) with the reduced/oxidized active material in the electrodes. Thus, salt hydrolysis plays a role that must be taken into account in the view of the larger complexity of the entire battery chemistry.

Conclusions

In this manuscript we tackled the analysis of the thermodynamics of hydrolysis in solvent media of four lithium salts used in lithium-ion batteries: $LiPF_6$, LiTFSI, LiFSI and LIFTFSI. We performed density functional theory calculations at the B3LYP/6–31++G** level of theory using an implicit solvation model, to derive the electronic structures, vibrational properties and the thermodynamic stability of reagents, reaction intermediates and hydrolysis products. Using these thermodynamic quantities, also combined with literature assessed values for solid phases like LiOH(s) and LiF(s), we outlined a realistic thermodynamic description of the tendency of

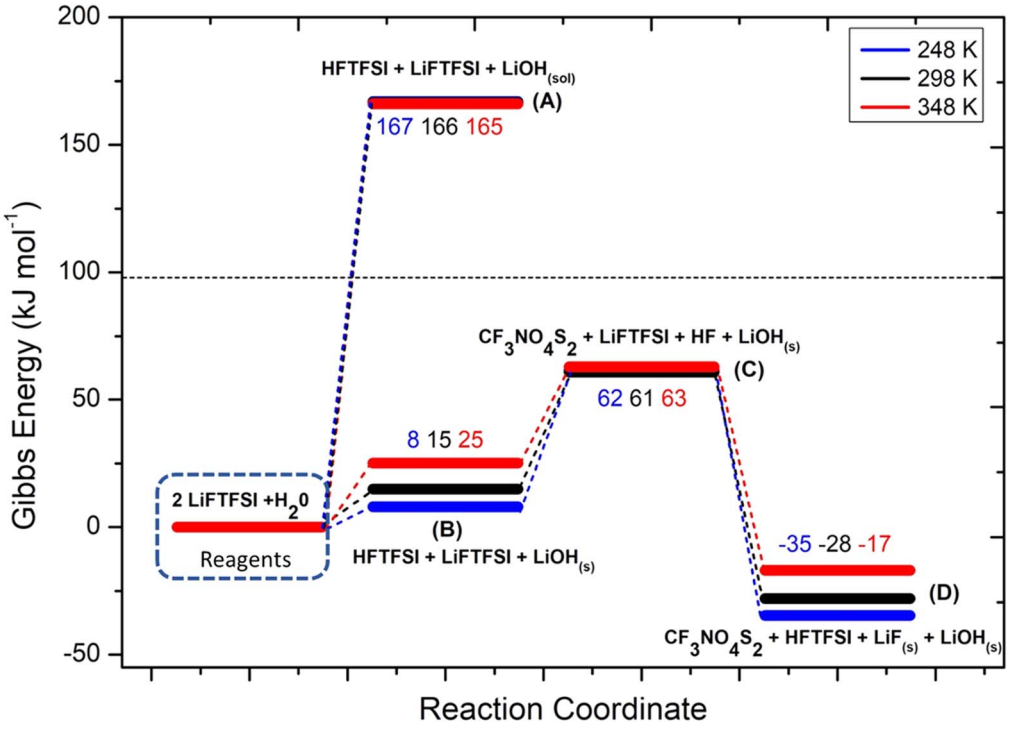

Figure 6. Potential Energy Surface (PES) of the LiFTFSI hydrolysis reaction, calculated at three temperatures (numerical values are the energy differences in respect to the initial state: i.e. 2LiFTFSI + H_2O at the various temperatures).

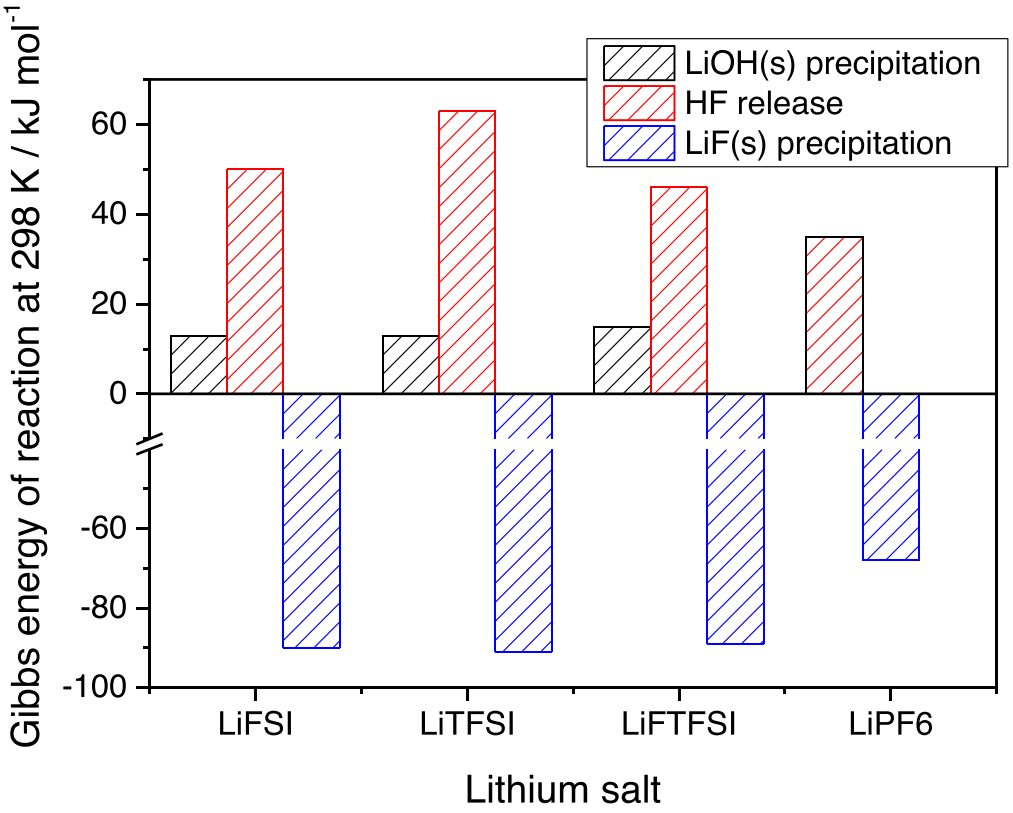

Figure 7. Comparison of the Gibbs energy of reactions of the three key-determining reactions in the lithium salt hydrolysis (note that the LiOH(s) precipitation and HF release steps occurs simultaneously in reaction 7b for $LiPF_6$).

these four salts to decompose by direct reaction with water following specific degradation paths. Our analysis has been performed at three different temperatures to account for the possible role played by the thermal effects. Overall, the use of imide-based anions limits the spontaneous hydrolysis, by hindering the formation of POF_3 that on the contrary largely occurs for $LiPF_6$. The hydrolyses of the (perfluroalkylsulfonyl)imide anions are driven by the precipitation of solid LiOH(s) and, to a lesser extent, of LiF(s). In particular,

LiTFSI apparently holds down more efficiently the precipitation of LiF(s) than the other anions and limits the onset of self-feeding salt degradation mechanisms.

Acknowledgments

The authors would like to acknowledge the financial support from the European UnionHorizon 2020 research and innovation programme within the Si-DRIVE project; grant agreement No. 814464.

ORCID

Sergio Brutti https://orcid.org/0000-0001-8853-9710

References

1. P. G. Kitz, P. Novák, and E. J. Berg, "Influence of water contamination on the SEI formation in Li-ion cells: an operando EQCM-D study." *ACS Appl. Mater. Interfaces*, **12**, 15934 (2020).
2. I. V. Veryovkin, C. E. Tripa, A. V. Zinovev, S. V. Baryshev, Y. Li, and D. P. Abraham, "TOF SIMS characterization of SEI layer on battery electrodes." *Nucl. Instrum. Methods Phys. Res., Sect. B*, **332**, 368 (2014).
3. K. L. Browning, L. Baggetto, R. R. Unocic, N. J. Dudney, and G. M. Veith, "Gas evolution from cathode materials: A pathway to solvent decomposition concomitant to SEI formation." *J. Power Sources*, **239**, 341 (2013).
4. J. Manzi and S. Brutti, "Surface chemistry on LiCoPO4 electrodes in lithium cells: SEI formation and self-discharge." *Electrochim. Acta*, **222**, 1839 (2016).
5. P. Lu, C. Li, E. W. Schneider, and S. J. Harris, "Chemistry, impedance, and morphology evolution in SEI films during formation in lithium ion batteries." *The Journal of Physical Chemistry C*, **118**, 896 (2013).
6. M. T. F. Rodrigues, C. Liao, K. Kalaga, I. A. Shkrob, and D. P. Abraham, "Dehydration rather than HF capture explains performance improvements of Li-Ion cells by ceramic nanoparticles." *ACS Appl. Energy Mater.*, **2**, 5380 (2019).
7. M. Agostini, A. Matic, S. Panero, F. Croce, R. Gunnella, P. Reale, and S. Brutti, "A mixed mechanochemical-ceramic solid-state synthesis as simple and cost effective route to high performing LNMO spinels." *Electrochim. Acta*, **235**, 262 (2017).
8. C. Yang, H. Tong, C. Luo, S. Yuan, G. Chen, and Y. Yang, "Boehmite particle coating modified microporous polyethylene membrane: A promising separator for lithium ion batteries." *J. Power Sources*, **348**, 80 (2017).
9. H. Lee et al., "A review of recent developments in membrane separators for rechargeable lithium-ion batteries." *Energy Environ. Sci.*, **7**, 3857 (2014).
10. R. Younesi, G. M. Veith, P. Johansson, K. Edström, and T. Vegge, "Lithium salts for advanced lithium batteries: Li–metal, Li–O2, and Li–S." *Energy Environ. Sci.*, **8**, 1905 (2015).
11. K. Ozawa, *Lithium Ion Rechargeable Batteries* (Wiley, New Jersey, NJ) (2009).
12. J. B. Goodenough and K. S. Park, "The Li-ion Rechargeable Battery: A Perspective." *J. Am. Chem. Soc.*, **135**, 1167 (2013).
13. Y. Yamada, J. Wang, S. Ko, E. Watanabe, and A. Yamada, *Nat. Energy*, **4**, 269 (2019).
14. T. Kawamura, S. Okada, and J. Yamaki, "Decomposition reaction of LiPF6-based electrolytes for lithium ion cells." *J. Power Sources*, **156**, 547 (2006).
15. C. Arbizzani, G. Gabrielli, and M. Mastragostino, "Thermal stability and flammability of electrolytes for lithium-ion batteries." *J. Power Sources*, **196**, 4801 (2011).
16. Q. Wang, L. Jiang, Y. Yu, and J. Sun, *Nano Energy*, **55**, 93 (2019).
17. A. Mauger, C. M. Julien, A. Paolella, M. Armand, and K. Zaghib, *Materials Science and Engineering R: Reports*, **134**, 1 (2018).
18. E. M. Wigayati, T. Lestariningsih, A. Subhan, C. R. Ratri, and I. Purawiardi, "Synthesis and characterization of LiBOB as electrolyte for lithium-ion battery." *Ionics*, **22**, 43 (2016).
19. S. R. Galle Kankanamge and D. G. Kuroda, "Molecular structure, chemical exchange, and conductivity mechanism of high concentration litfsi electrolytes." *J. Phys. Chem. B*, **124**, 1965 (2020).
20. M. Montanino, S. Passerini, and G. B. Appetecchi, *Rechargeable Lithium Batteries: From Fundamentals to Applications* (Elsevier)73 (2015).
21. C. G. Barlow, "Reaction of water with hexafluorophosphates and with Li bis (perfluoroethylsulfonyl)imide salt." *Electrochem. Solid-State Lett.*, **2**, 362 (1999).
22. M. Stich, M. Göttlinger, M. Kurniawan, U. Schmidt, and A. Bund, "Hydrolysis of LiPF6 in carbonate-based electrolytes for lithium-ion batteries and in aqueous media." *J. Phys. Chem. C*, **122**, 8836 (2018).
23. K. Tasaki, K. Kanda, S. Nakamura, and M. Ue, "Decomposition of LiPF6 and Stability of PF5 in Li-Ion Battery Electrolytes." *J. Electrochem. Soc.*, **150**, A1628 (2003).
24. Y. Lu, F. L. King, and D. C. Duckworth, "Electrochemically-induced reactions of hexafluorophosphate anions with water in negative ion electrospray mass spectrometry of undiluted ionic liquids." *J. Am. Soc. Mass. Spectrom.*, **17**, 939 (2006).
25. S. Solchenbach, M. Metzger, M. Egawa, H. Beyer, and H. A. Gasteiger, "Quantification of PF 5 and POF 3 from side reactions of LiPF 6 in li-ion batteries." *J. Electrochem. Soc.*, **165**, A3022 (2018).
26. C. Xu, G. Hernández, S. Abbrent, L. Kobera, R. Konefal, J. Brus, K. Edström, D. Brandell, and J. Mindemark, "Unraveling and mitigating the storage instability of fluoroethylene carbonate-containing LiPF6 electrolytes to stabilize lithium metal anodes for high-temperature rechargeable batteries." *ACS Appl. Energy Mater.*, **2**, 4925 (2019).
27. P. Verma, P. Maire, and P. Novák, "A review of the features and analyses of the solid electrolyte interphase in Li-ion batteries." *Electrochim. Acta*, **55**, 6332 (2010).
28. D. Aurbach, B. Markovsky, G. Salitra, E. Markevich, Y. Talyossef, M. Koltypin, L. Nazar, B. Ellis, and D. Kovacheva, "Review on electrode-electrolyte solution interactions, related to cathode materials for Li-ion batteries." *J. Power Sources*, **165**, 491 (2007).
29. S. F. Lux, I. T. Lucas, E. Pollak, S. Passerini, M. Winter, and R. Kostecki, "The mechanism of HF formation in LiPF6 based organic carbonate electrolytes." *Electrochem. Commun.*, **14**, 47 (2012).
30. J. G. Han, M. Y. Jeong, K. Kim, C. Park, C. H. Sung, D. W. Bak, K. H. Kim, K. M. Jeong, and N. S. Choi, "An electrolyte additive capable of scavenging HF and PF5 enables fast charging of lithium-ion batteries in LiPF6-based electrolytes." *J. Power Sources*, **446**, 227366 (2020).
31. D. Strmcnik et al., "Electrocatalytic transformation of HF impurity to H2 and LiF in lithium-ion batteries." *Nat. Catal.*, **1**, 255 (2018).
32. J. Wojciechowski, Ł. Kolanowski, A. Bund, and G. Lota, "The influence of current collector corrosion on the performance of electrochemical capacitors." *J. Power Sources*, **368**, 18 (2017).
33. M. Morita, T. Shibata, N. Yoshimoto, and M. Ishikawa, "Anodic behavior of aluminum in organic solutions with different electrolytic salts for lithium ion batteries." *Electrochim. Acta*, **47**, 2787 (2002).
34. E. Cho, J. Mun, O. B. Chae, O. M. Kwon, H. T. Kim, J. H. Ryu, Y. G. Kim, and S. M. Oh, "Corrosion/passivation of aluminum current collector in bis(fluorosulfonyl) imide-based ionic liquid for lithium-ion batteries." *Electrochem. Commun.*, **22**, 1 (2012).
35. Y. Shao et al., "Advances in methods and algorithms in a modern quantum chemistry program package." *Phys. Chem. Chem. Phys.*, **8**, 3172 (2006).
36. T. Yanai, D. P. Tew, and N. C. Handy, "A new hybrid exchange–correlation functional using the Coulomb-attenuating method (CAM-B3LYP)." *Chemical Physics Letters*, **393**, 51 (2004).
37. A. D. McLean and G. S. Chandler, "Contracted Gaussian basis sets for molecular calculations. I. Second row atoms, Z = 11–18." *J. Chem. Phys.*, **72**, 5639 (1980).
38. M. Cossi, N. Rega, G. Scalmani, and V. Barone, "Energies, structures, and electronic properties of molecules in solution with the C-PCM solvation model." *J. Comput. Chem.*, **24**, 669 (2003).
39. M. Frisch, *Gaussian 09* (Gaussian, Inc., Wallingford, CT) (2009).
40. Y. Zhao and D. G. Truhlar, "The M06 suite of density functionals for main group thermochemistry, thermochemical kinetics, noncovalent interactions, excited states, and transition elements: Two new functionals and systematic testing of four M06-class functionals and 12 other function." *Theor. Chem. Acc.*, **120**, 215 (2008).
41. J.-D. Chai and M. Head-Gordon, "Long-range corrected hybrid density functionals with damped atom–atom dispersion corrections." *Phys. Chem. Chem. Phys.*, **10**, 6615 (2008).
42. S. Grimme, "Improved second-order Møller-Plesset perturbation theory by separate scaling of parallel- and antiparallel-spin pair correlation energies." *J. Chem. Phys.*, **118**, 9095 (2003).
43. E. Mourad et al., "Singlet oxygen from cation driven superoxide disproportionation and consequences for aprotic metal-O2 batteries." *Energy Environ. Sci.*, **12**, 2559 (2019).
44. M. W. Chase Jr, "NIST-janaf thermochemical tables." *J. Phys. Chem. Ref. Data*, Monograph, 1510 (1998).
45. S. Solchenbach, M. Metzger, M. Egawa, H. Beyer, and H. A. Gasteiger, "Quantification of PF 5 and POF 3 from side reactions of LiPF 6 in Li-Ion batteries." *J. Electrochem. Soc.*, **165**, A3022 (2018).
46. K. Tasaki, K. Kanda, S. Nakamura, and M. Ue, "Decomposition of LiPF[sub 6] and stability of PF[sub 5] in Li-Ion battery electrolytes." *J. Electrochem. Soc.*, **150**, A1628 (2003).
47. S. E. Sloop, J. K. Pugh, S. Wang, J. B. Kerr, and K. Kinoshita, "Chemical reactivity of PF5 and LiPF6 in ethylene carbonate/dimethyl carbonate solutions." *Electrochem. Solid-State Lett.*, **4**, A42 (2001).
48. K. Kondo, M. Sano, A. Hiwara, T. Omi, M. Fujita, A. Kuwae, M. Iida, K. Mogi, and H. Yokoyama, "Conductivity and solvation of Li + Ions of LiPF6 in propylene carbonate solutions." *J. Phys. Chem. B*, **104**, 5040 (2000).